Electronic Supplementary Material (ESI) for Journal of Materials Chemistry C.

SUPPORTING INFORMATION

Complementary Electrochromic Device via A Scalable Solution Process: A Step Towards Affordable and Energy-Efficient Smart Windows

Pritha Dutta[a,b], Indrajit Mondal[c], Aalekhya Saha[a], Ashutosh K. Singh[,a,b,d]*

[a]*Centre for Nano and Soft Matter Sciences, Bangalore 562162, India.*

[b]*Manipal Academy of Higher Education, Manipal 576104, Karnataka, India.*

[c]*Chemistry & Physics of Materials Unit, Jawaharlal Nehru Centre for Advanced Scientific Research, Bangalore, Karnataka, 560064, India*

[d]*Academy of Scientific and Innovative Research (AcSIR), Ghaziabad, Uttar Pradesh, 201002, India*

*Corresponding author

E-mail addresses: Dr. Ashutosh K. Singh (aksingh@cens.res.in, ashuvishen@gmail.com)

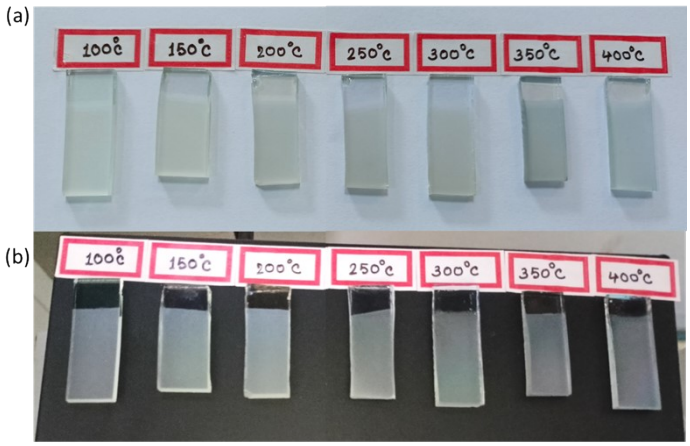

Figure S1. Digital images of the W-films synthesized at different temperatures, shown in (a) white background and (b) black background.

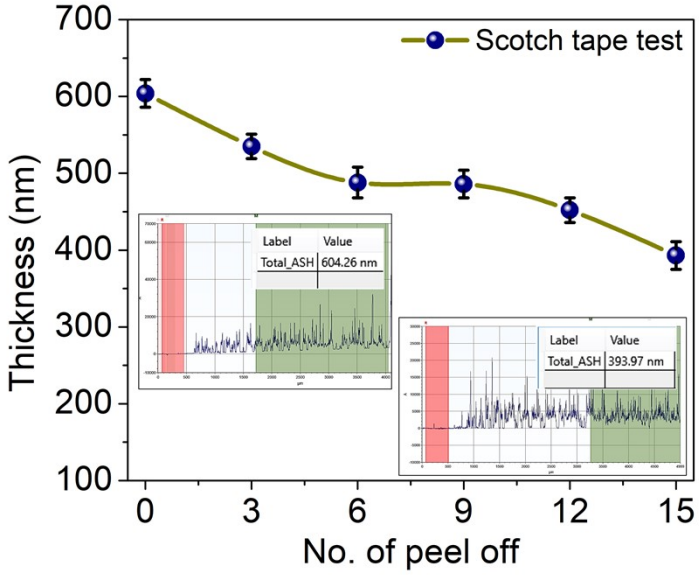

Figure S2. Adhesion test of the film by scotch tape. Inset images correspond to the stylus profiles with the mentioned thicknesses for the pristine film and the film after 15 numbers of peel-off.

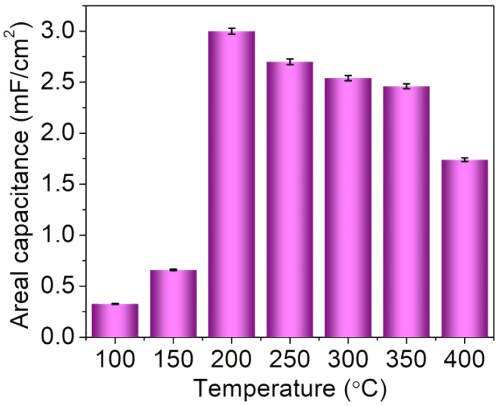

Figure S3. The variation in areal capacitances of W-films synthesized at different temperatures.

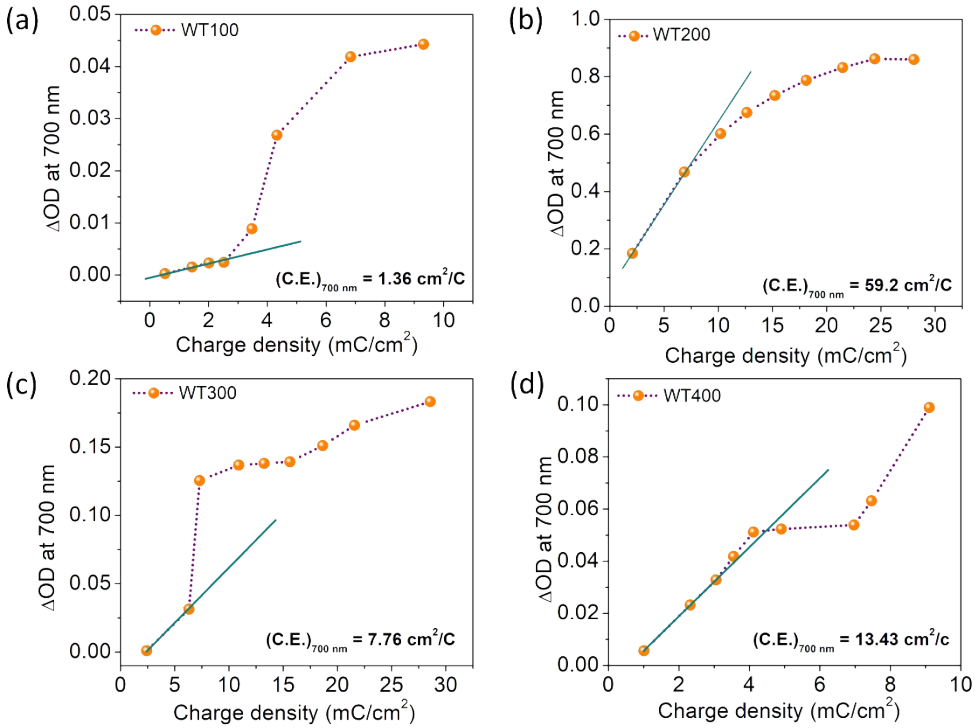

Figure S4. ΔOD vs charge density plots to calculate coloration efficiencies (C.E.) of (a) WT100, (b) WT200, (c) WT300, and (d) WT400.

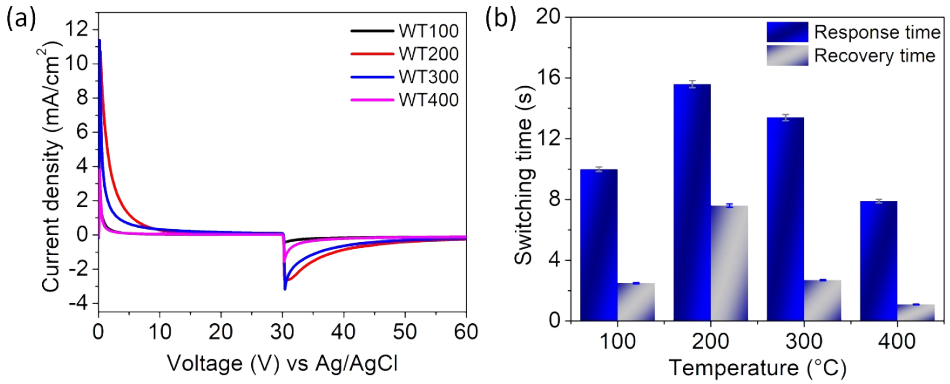

Figure S5. (a) Chronoamperometry curves and (b) bar diagram for switching times of W-films synthesized at different temperatures.

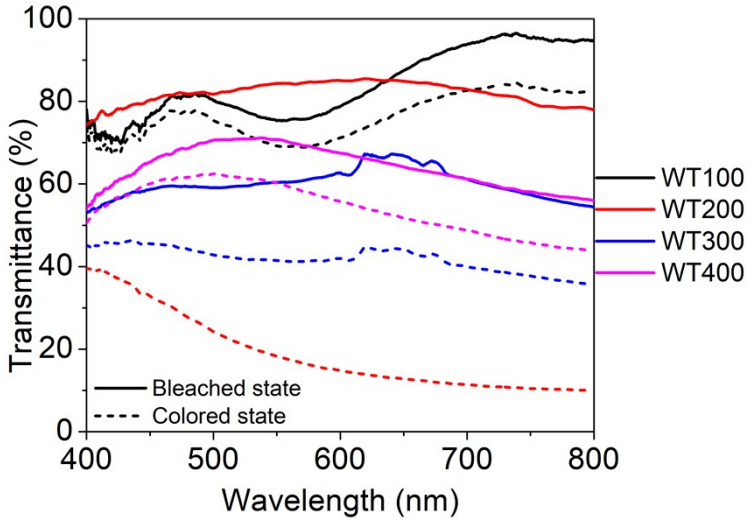

Figure S6. Transmittance spectra of the W-films synthesized at different temperatures for bleached and colored states.

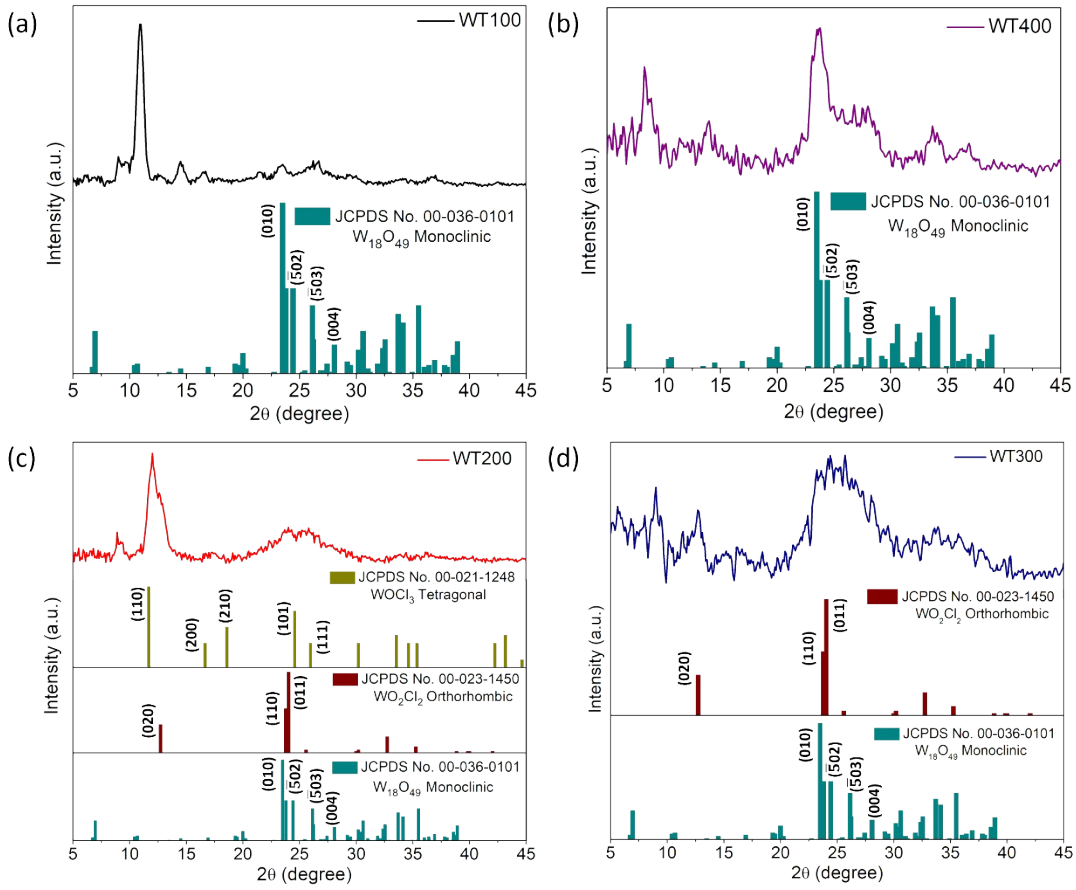

Figure S7. XRD patterns of the films (a) WT100, (b) WT400, (c) WT200, and (d) WT300 with the respective JCPDS reference patterns.

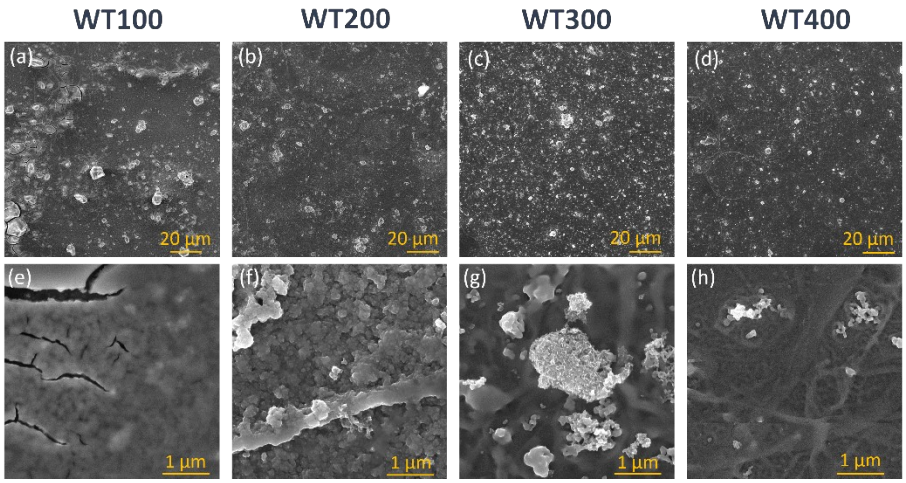

Figure S8. Morphological variations through FESEM images of (a,e) WT100, (b,f) WT200, (c,g) WT300, and (d,h) WT400 in low and high magnifications.

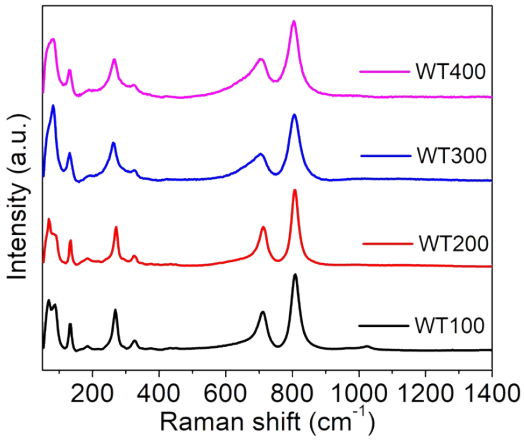

Figure S9. Raman spectra of W-films synthesized at different temperatures.

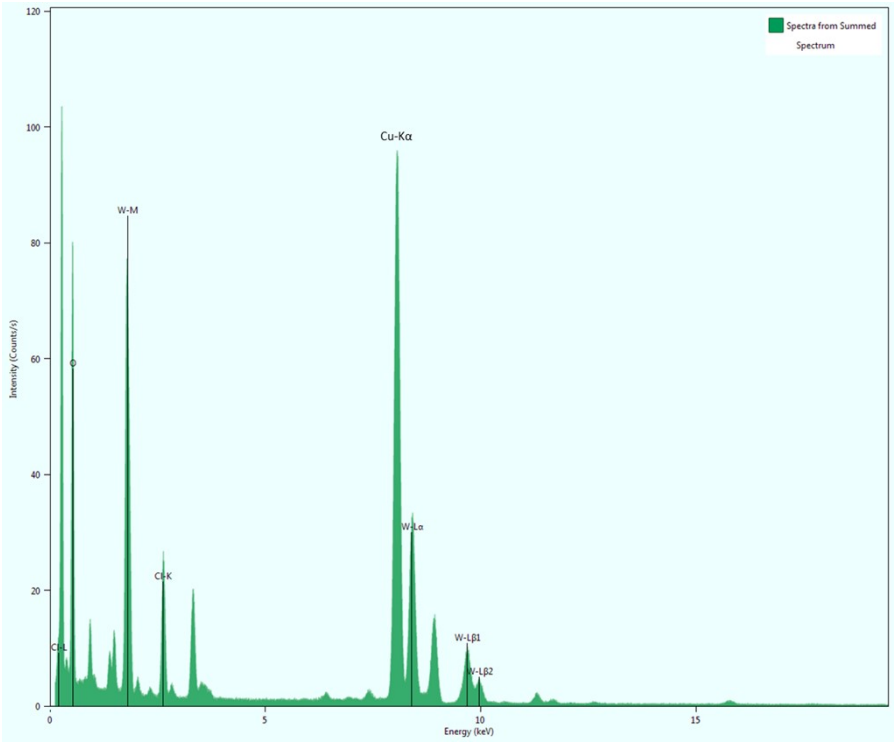

Figure S10. EDAX analysis through TEM for WT200.

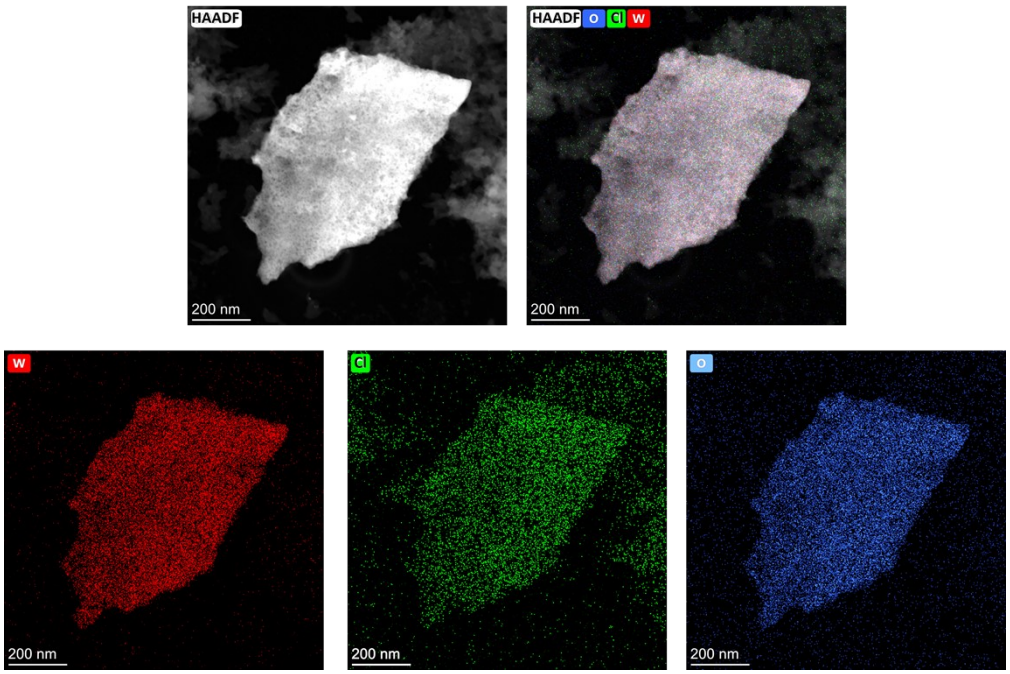

Figure S11. Elemental mapping from TEM for WT200.

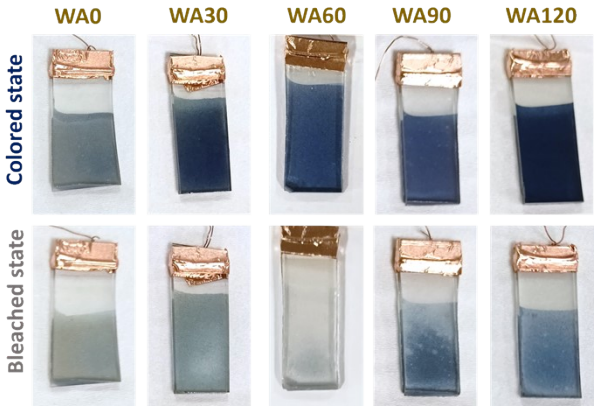

Figure S12. Photographs of W-films vacuum-annealed for different times in colored and bleached states.

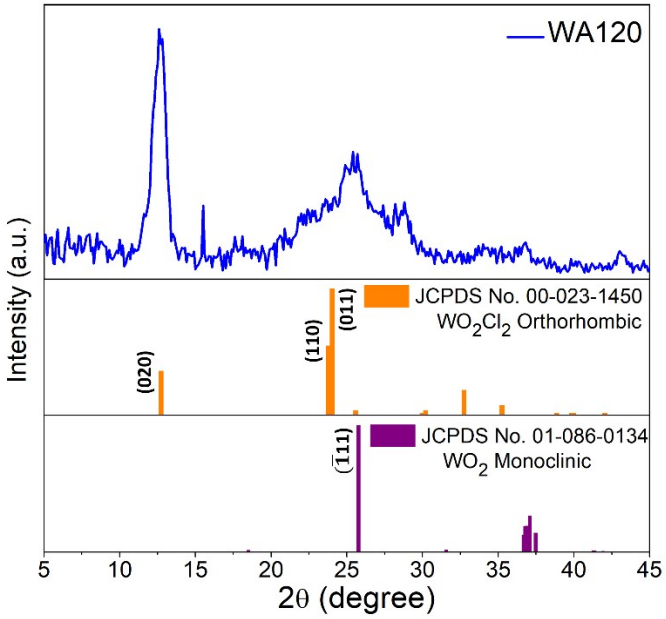

Figure S13. XRD patterns of the film WA120 with the respective JCPDS reference patterns.

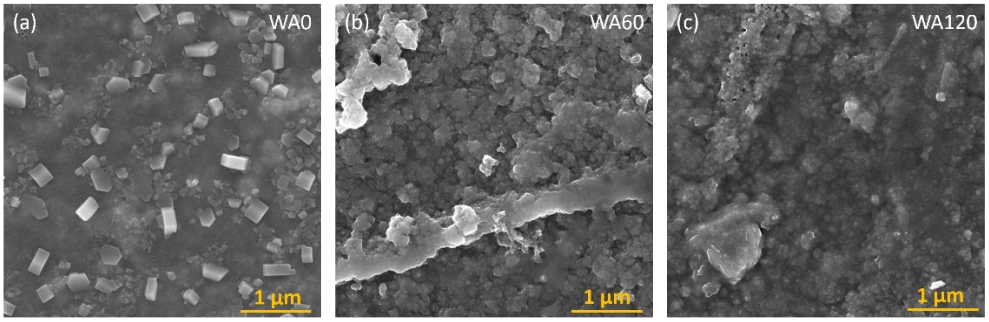

Figure S14. Morphological variations through FESEM images of (a) WA0, (b) WA60, and (c) WA120 in 30kX magnification.

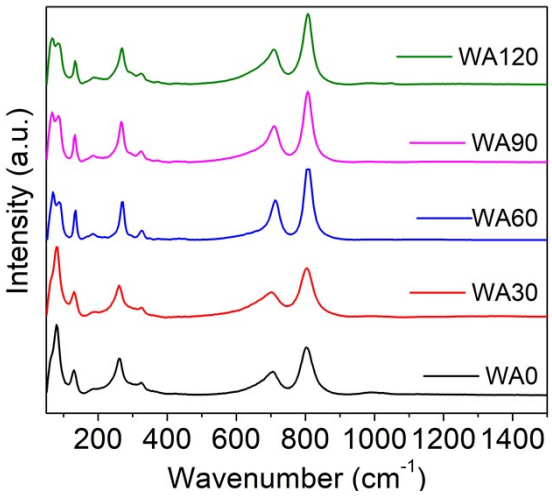

Figure S15. Variation in Raman spectra of W-films vacuum-annealed for different times.

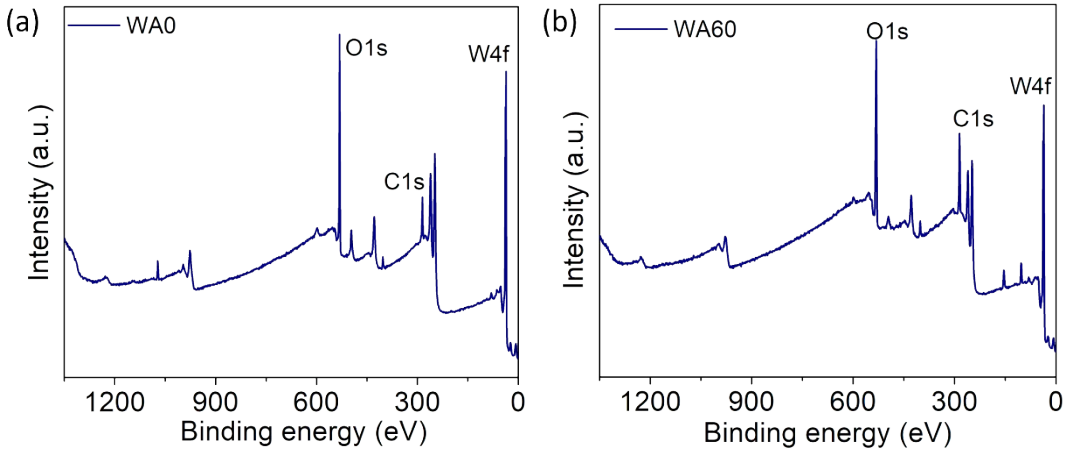

Figure S16. XPS Survey spectra for the samples (a) WA0 and (b) WA60.

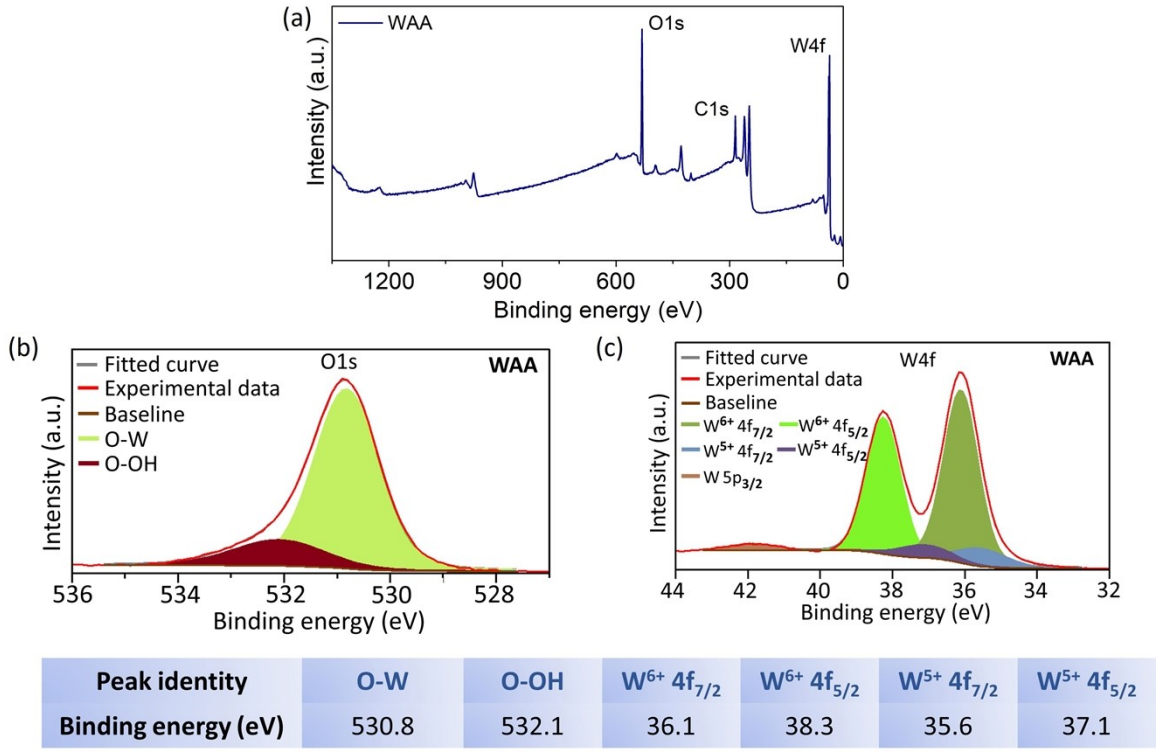

Peak identity	O-W	O-OH	W^{6+} $4f_{7/2}$	W^{6+} $4f_{5/2}$	W^{5+} $4f_{7/2}$	W^{5+} $4f_{5/2}$
Binding energy (eV)	530.8	532.1	36.1	38.3	35.6	37.1

Figure S17. XPS (a) survey spectrum, (b) O1s, and (b) W4f core-level spectra of WAA. The table indicates the positions of different peaks from (b) O1s and (c) W4f spectra.

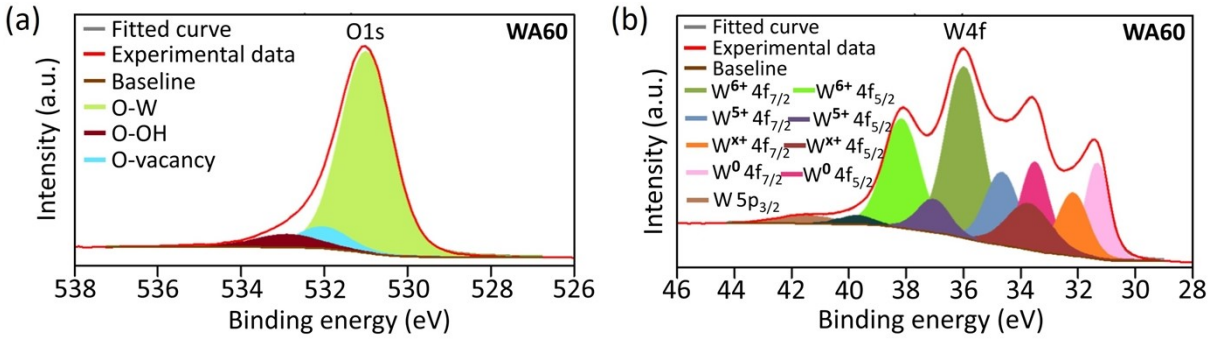

Figure S18. Core-level XPS spectra of (a) O1s and (b) W4f for, after surface etching of the sample WA60.

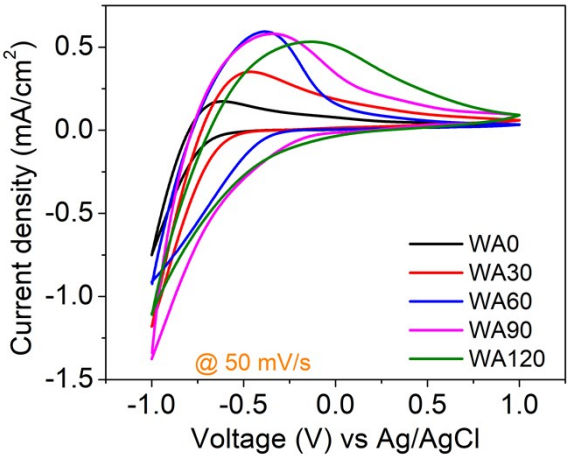

Figure S19. CVs at 50 mV/s scan rate of W-films vacuum-annealed for different times.

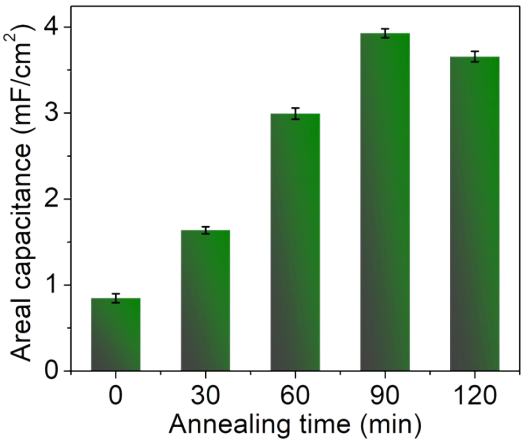

Figure S20. Bar diagram for areal capacitances of W-films vacuum-annealed for different times.

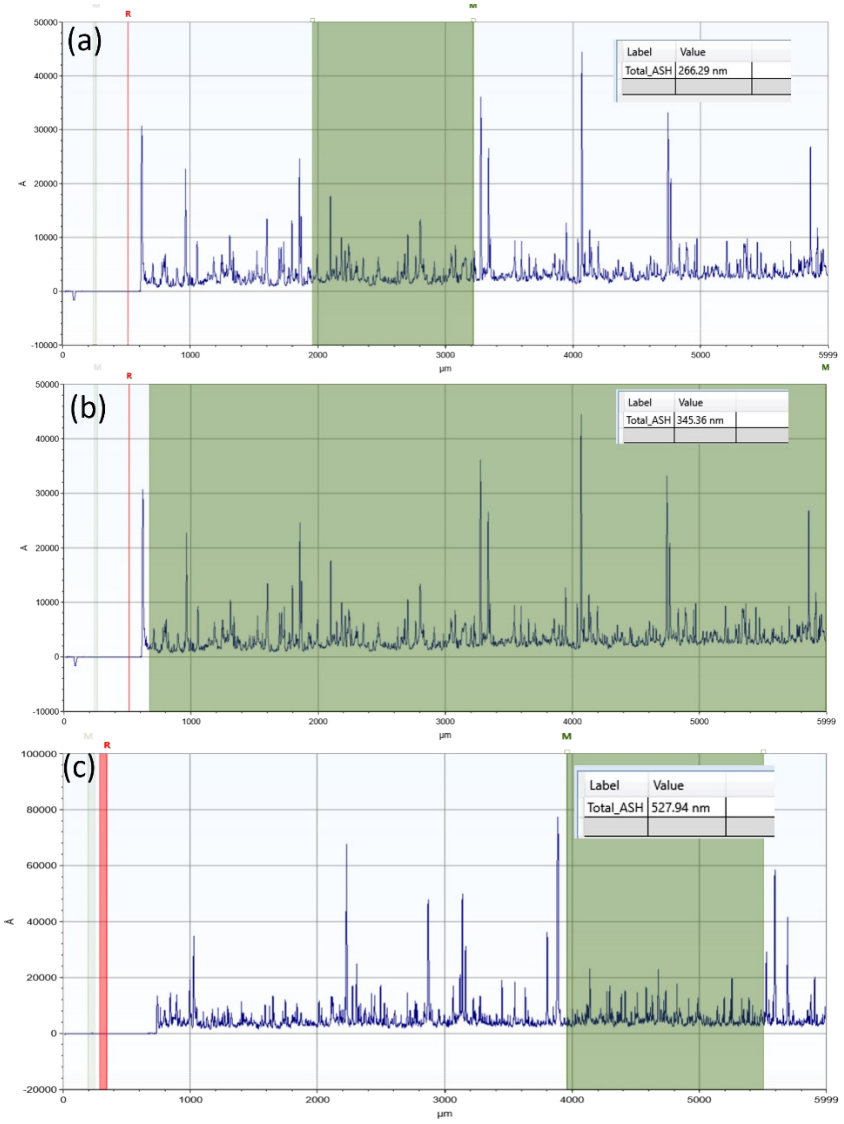
(a)
Label
Value
Total_ASH
266.29 nm
(b)
Label
Value
Total_ASH
345.36 nm
(c)
Label
Value
Total_ASH
527.94 nm
A
µm
R
M

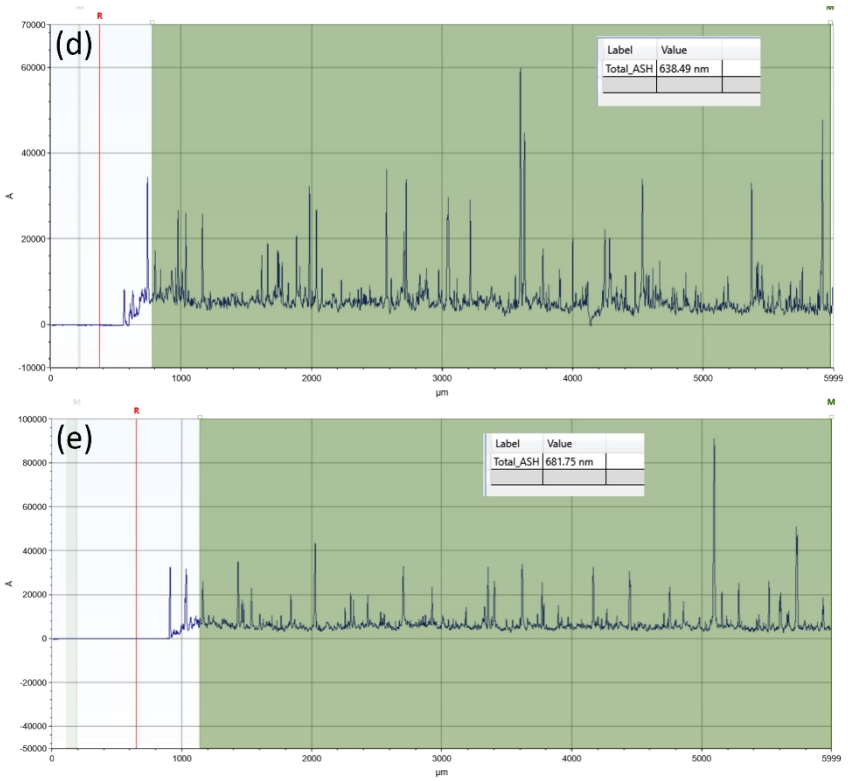

Figure S21. Surface profiling thickness analysis for the samples (a) WW230, (b) WW345, (c) WW502, (d) WW630, and (e) WW680. For all the tables in inset images, "Total_ASH" defines the thickness in nm.

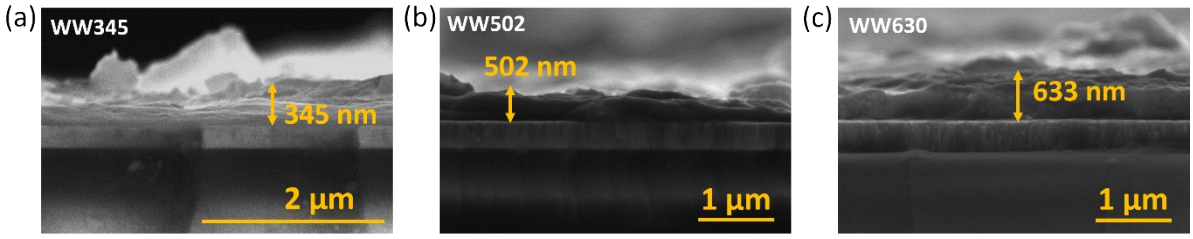

Figure S22. Thickness measurements through cross-sectional FESEM images of (a) WW345, (b) WW502, and (c) WW630.

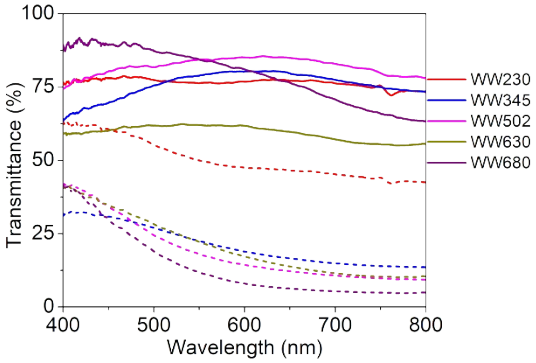

Thickness of the film (nm)	Optical modulation (%) at	
	550 nm	700 nm
230	26.4	31
345	56.36	62.59
502	66.1	71.5
630	39.82	45.6
680	72.6	65.33

Figure S23. The transmittance spectra of the samples deposited in different thicknesses. The table defines the optical modulations for all the samples with different thicknesses at two wavelengths.

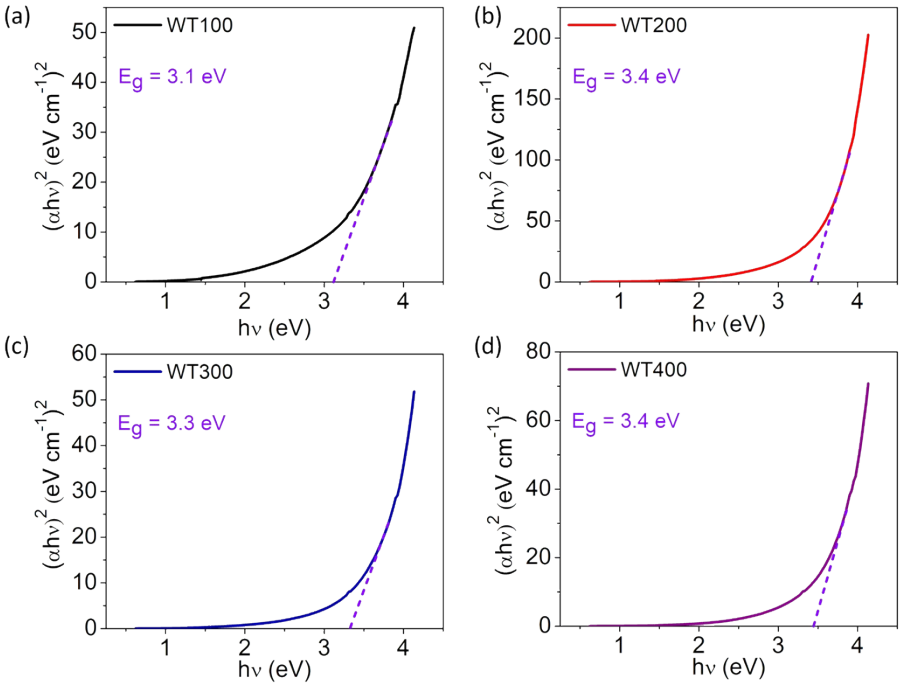

Figure S24: Tauc plots for (a) WT100, (b) WT200, (c) WT300, and (d) WT400.

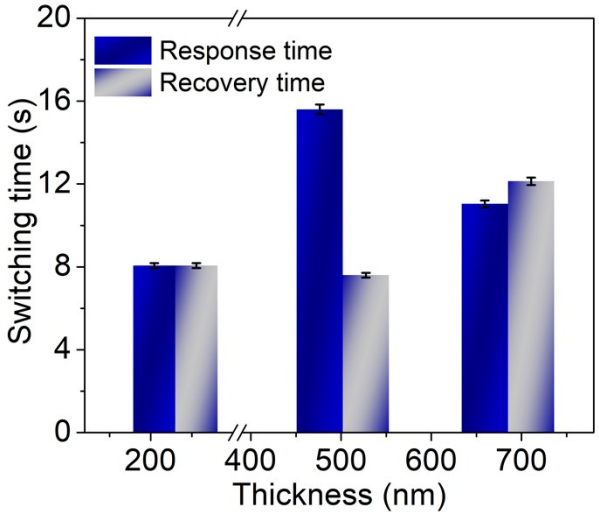

Figure S25. Bar diagram for switching time of WW230, WW502, and WW680.

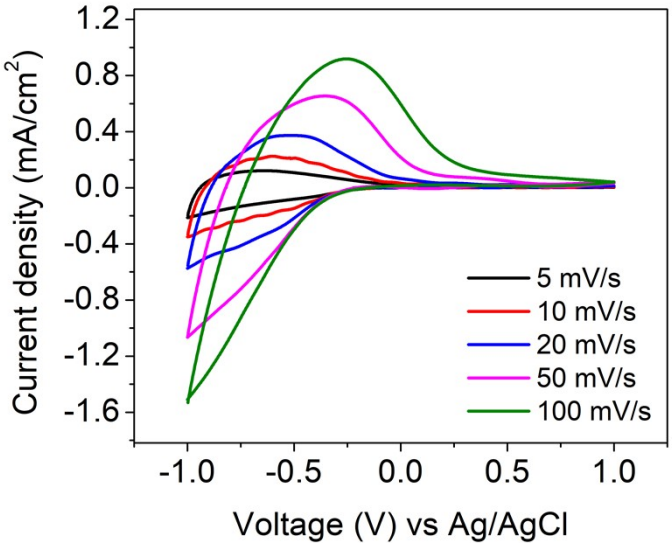

Figure S26. The CV of the W-film deposited with optimized parameters at different scan rates.

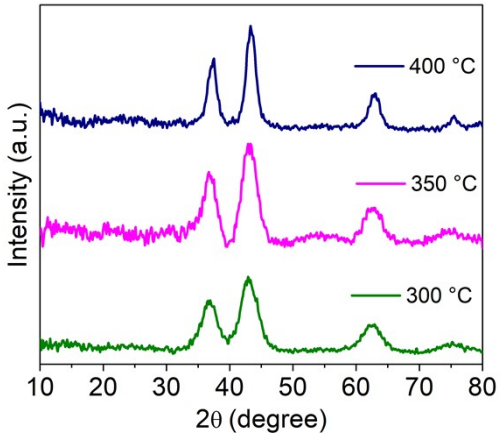

Figure S27. XRD patterns of the NiO film, deposited at different temperatures.

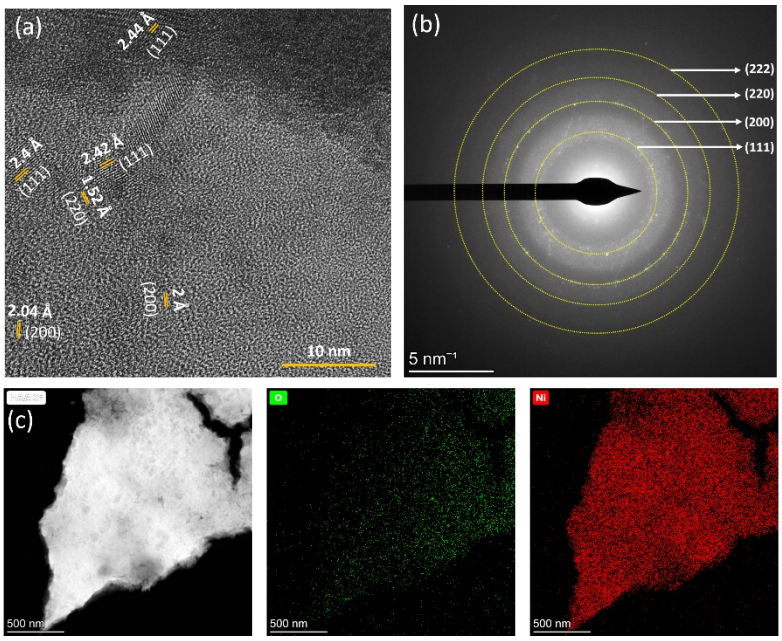

Figure S28. (a) HRTEM, (b) SAED pattern, (c) HAADF-TEM image and corresponding elemental maps for NiO film.

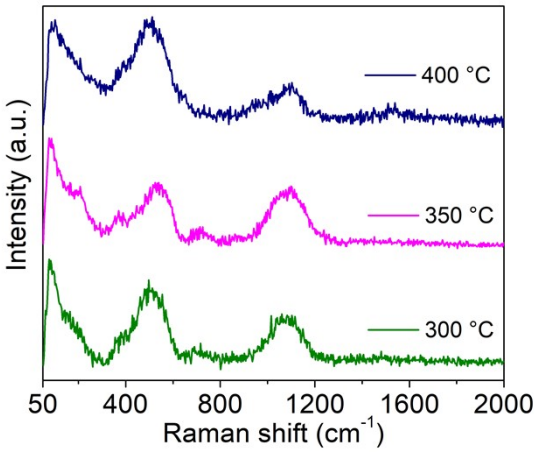

Figure S29. Raman spectra of NiO film deposited at different temperatures.

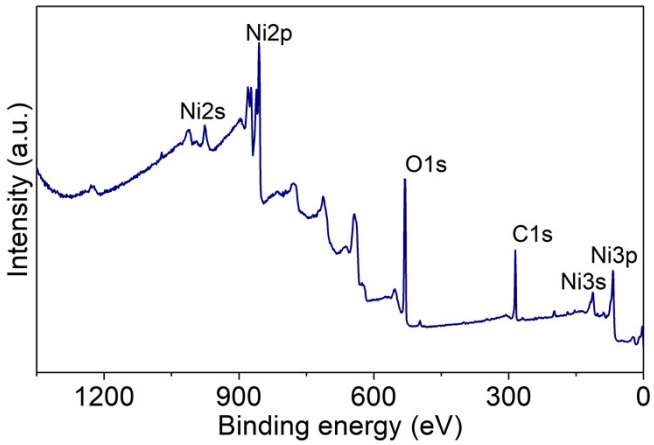

Figure S30. XPS survey spectrum of NiO film.

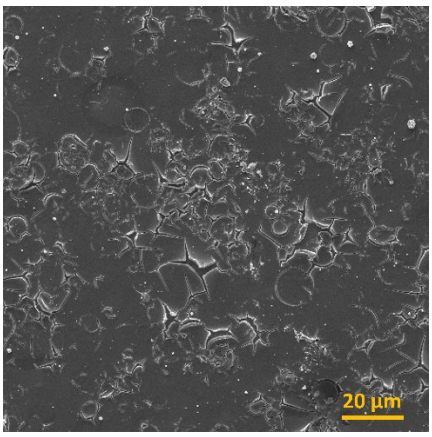

Figure S31. FESEM image of the NiO film at 1kX magnification.

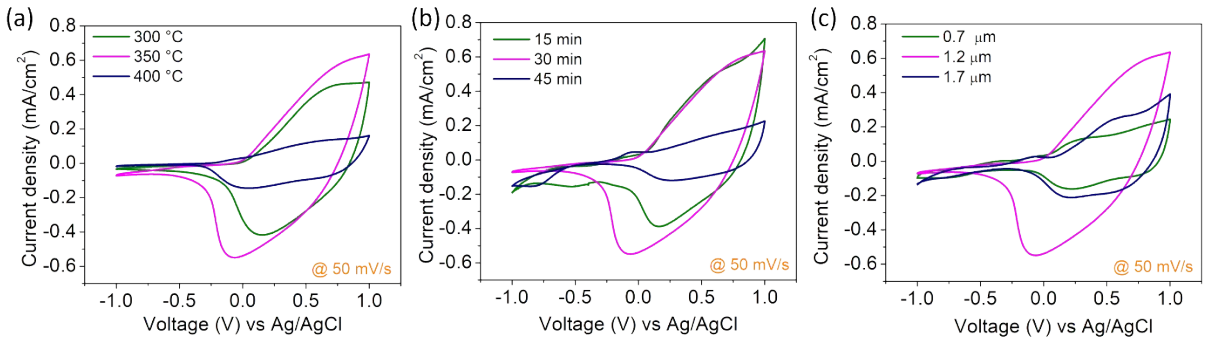

Figure S32. CV at 50 mV/s scan rate of NiO films, deposited at (a) different temperatures, annealed for (b) different times, and deposited in (c) different thicknesses.

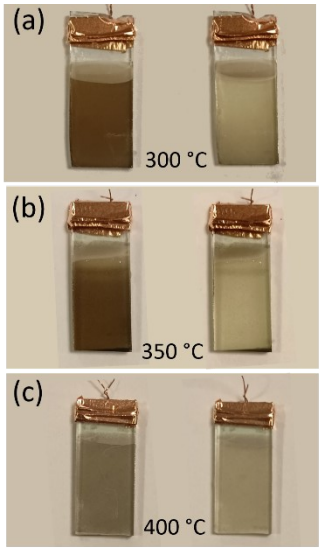

Figure S33. Digital images in colored and bleached states of NiO films, deposited at the temperature of (a) 300 °C, (b) 350 °C, and (c) 400 °C.

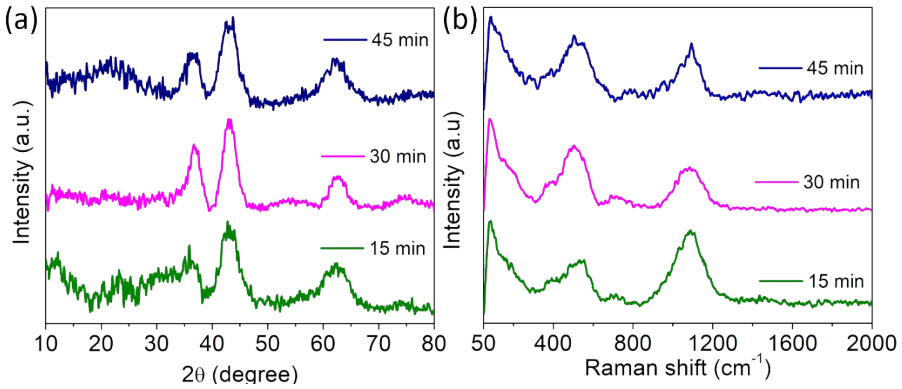

Figure S34. (a) XRD patterns and (b) Raman spectra of NiO films, annealed at different times.

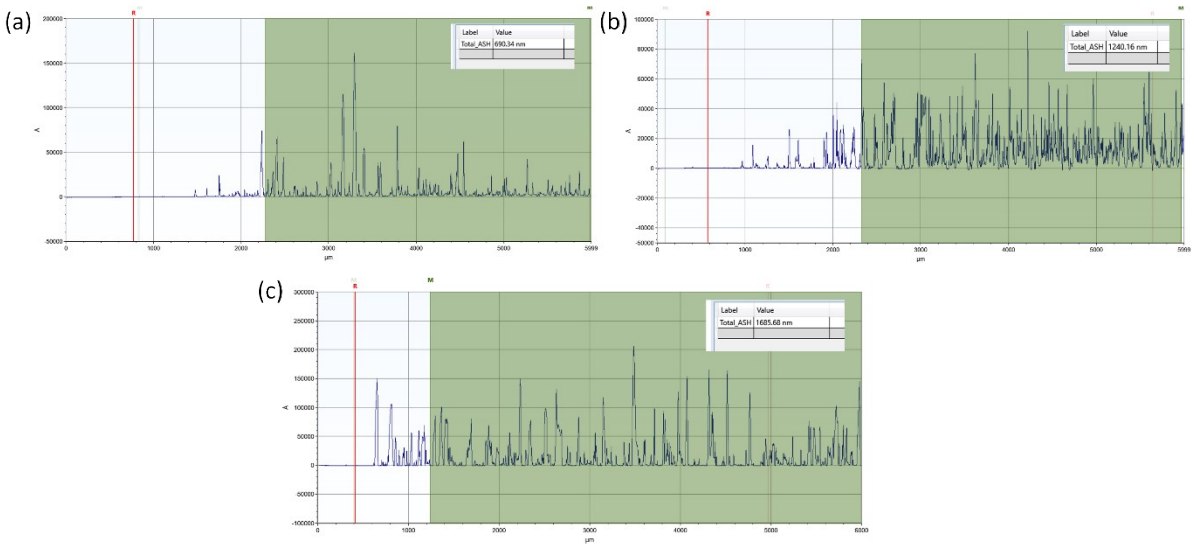

Figure S35. Surface profiling thickness analysis for the NiO films deposited with the thickness of (a) 0.7 µm, (b) 1.2 µm, and (c) 1.7 µm.

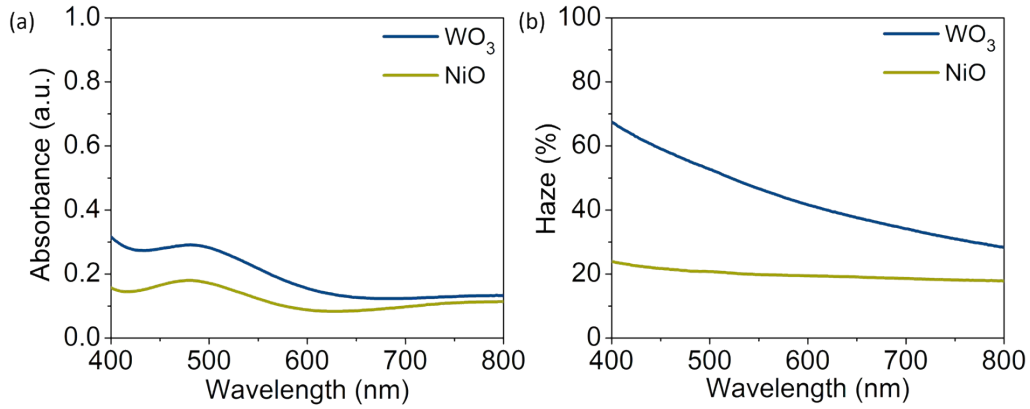

Figure S36. (a) Absorbance, and (b) Haze measurements for both WO_3 and NiO electrodes.

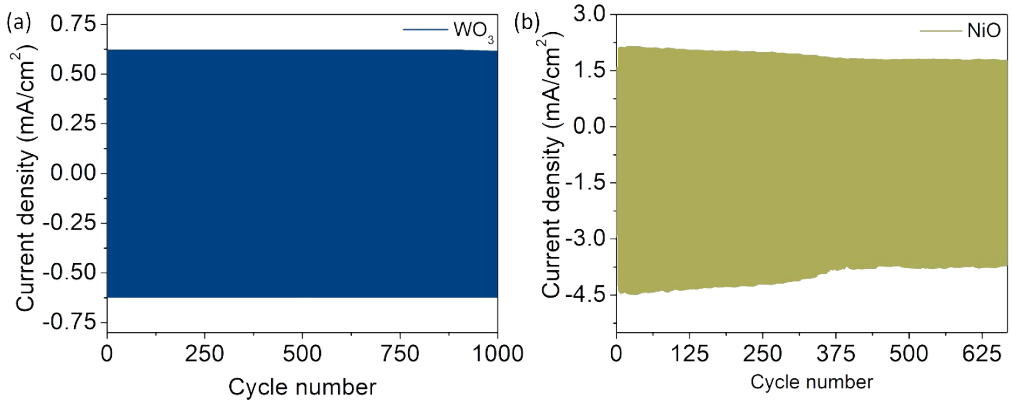

Figure S37. Cycling stability test through chronoamperometry of (a) optimized W-film for 1000 cycles and (b) the optimized NiO film for 670 cycles.

Figure S38. The assembled complementary electrochromic device picture before filling the electrolyte into it.

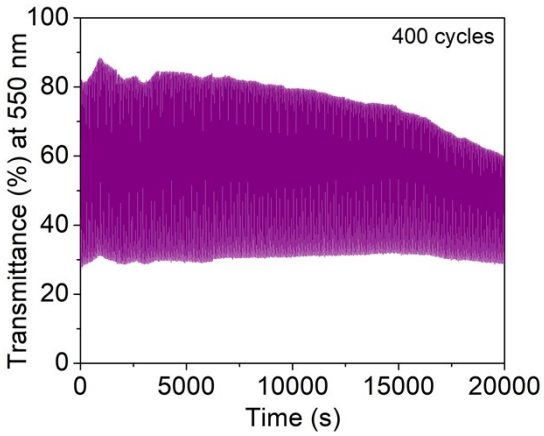

Figure S39. Cycling stability test of the electrochromic device through measuring in-situ transmittance spectra at 550 nm for 400 cycles.

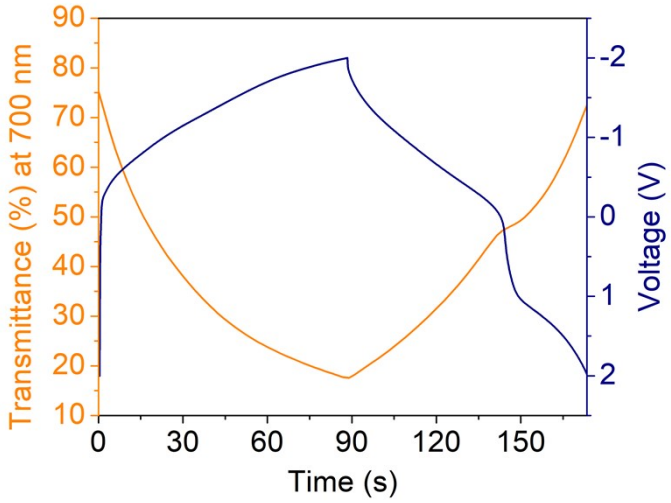

Figure S40. Galvanostatic charge-discharge curve at 0.1 mA/cm^2 and the corresponding optical response at 700 nm of the electrochromic device.

Complementary Electrochromic Device	Deposition method	Optical modulation	Switching time	Coloration efficiency (cm²/C)	Reference
WO_3/NiO	E-beam evaporation	54.6% at 550 nm	-	153	1
WO_3/NiO	Sol-gel	84% at 700 nm	T_c = 10 s, T_b = 11.7 s	55.2	2
WO_3/NiO	Sputtering and chemical bath deposition	55% at 550 nm	T_c = 10 s, T_b = 20 s	87	3
WO_3/NiO	Cathodic arc plasma	46% at 633 nm	T_c = 4.6 s, T_b = 3.1 s	90	4
WO_3/NiO	**Direct spray coating of precursor**	**59.2% at 700 nm and 67% at 550 nm**	**T_c = 10.1 s, T_b = 17.2 s**	**102.7 at 700 nm and 81.6 at 550 nm**	**This work**

Table 1: Performance comparison of direct spray-coated WO_3/NiO based CECD with WO3-NiO-based CECD using other coating methods.

References:

1. L. Wang, X. Zhang and Y. Li, *ACS Sustain Chem Eng*, 2023, **11**, 13566–13573.
2. M. Rakibuddin, M. A. Shinde and H. Kim, *Ceram Int*, 2020, **46**, 8631–8639.
3. J. Zhang, J. P. Tu, X. H. Xia, Y. Qiao and Y. Lu, *Solar Energy Materials and Solar Cells*, 2009, **93**, 1840–1845.
4. P. W. Chen, C. Te Chang, T. F. Ko, S. C. Hsu, K. D. Li and J. Y. Wu, *Sci Rep*, 2020, **10**, 8430.